MucosalImmunology

www.nature.com/mi

ARTICLE

A novel role for C–C motif chemokine receptor 2 during infection with hypervirulent *Mycobacterium tuberculosis*

Micah D. Dunlap[1,2], Nicole Howard[1], Shibali Das[1], Ninecia Scott[1], Mushtaq Ahmed[1], Oliver Prince[1], Javier Rangel-Moreno[3], Bruce A. Rosa[4], John Martin[4], Deepak Kaushal[5], Gilla Kaplan[6], Makedonka Mitreva[4], Ki-Wook Kim[2], Gwendalyn J. Randolph[2] and Shabaana A. Khader[1,2]

C–C motif chemokine receptor 2 (CCR2) is a major chemokine axis that recruits myeloid cells including monocytes and macrophages. Thus far, $CCR2^{-/-}$ mice have not been found to be susceptible to infection with *Mycobacterium tuberculosis* (*Mtb*). Here, using a prototype W-Beijing family lineage 2 *Mtb* strain, HN878, we show that $CCR2^{-/-}$ mice exhibit increased susceptibility to tuberculosis (TB). Following exposure to *Mtb* HN878, alveolar macrophages (AMs) are amongst the earliest cells infected. We show that AMs accumulate early in the airways following infection and express CCR2. During disease progression, CCR2-expressing AMs exit the airways and localize within the TB granulomas. RNA-sequencing of sorted airway and non-airway AMs from infected mice show distinct gene expression profiles, suggesting that upon exit from airways and localization within granulomas, AMs become classically activated. The absence of $CCR2^{+}$ cells specifically at the time of AM egress from the airways resulted in enhanced susceptibility to *Mtb* infection. Furthermore, infection with an *Mtb* HN878 mutant lacking phenolic glycolipid (PGL) expression still resulted in increased susceptibility in $CCR2^{-/-}$ mice. Together, these data show a novel role for CCR2 in protective immunity against clinically relevant *Mtb* infections.

Mucosal Immunology (2018) 11:1727–1742; https://doi.org/10.1038/s41385-018-0071-y

INTRODUCTION

Mycobacterium tuberculosis (*Mtb*), the causative agent of pulmonary tuberculosis (TB), infects approximately one-third of the world's population and results in 1.4 million deaths annually[1]. *Mycobacterium bovis* bacillus Calmette-Guérin is the only licensed vaccine against TB, however it is not very effective at protecting against adult pulmonary TB. A major hurdle in the design of new and effective vaccines against TB is our poor understanding of the early immune mechanisms mediating protective immunity against *Mtb* infection.

A major chemokine axis that recruits innate immune cells to the lungs is the C–C motif chemokine receptor 2 (CCR2). $CCR2^{-/-}$ mice aerosol-infected with Euro-American lineage 4 *Mtb* strains showed defective accumulation of myeloid dendritic cell (mDC) and macrophage/monocyte populations in the *Mtb*-infected lung, with coincident delayed T cell responses.[2,3] Despite decreased innate cellular recruitment, $CCR2^{-/-}$ mice were surprisingly not more susceptible to *Mtb* infection,[2] propagating the idea that the CCR2 axis is dispensable for protective immunity to infection with *Mtb*.[4]

A major ligand for CCR2 is C–C motif chemokine ligand 2 (CCL2), along with the ligands CCL7 and CCL12. In human populations, meta-analysis of the identified −2518 A/G single nucleotide polymorphism (SNP) in the promoter region of the CCL2 gene show significantly elevated risk for pulmonary TB.[5] Recent studies have highlighted differences in cytokine induction and immune requirements for *Mtb* control to be dependent on the infecting *Mtb* strain.[6,7] Studies using the zebrafish granuloma model have described that *Mycobacterium marinum* expressing virulence factors such as PGLs drive increased expression of CCL2, and mediate recruitment of $CCR2^{+}$ permissive monocytes to promote pathogenesis.[8,9] Thus, murine studies suggest a dispensable role for CCR2, zebrafish and *M. marinum* infection models suggest a pathological role for CCR2, while human studies propose a critical but as yet undefined role for the ligand, CCL2.

Alveolar macrophages (AMs) are tissue-resident phagocytes localized to the airway and are believed to be the first contact and primary reservoir for replication of *Mtb* following inhalation of the bacteria.[10,11] During acute *Mtb* infection, AMs can exacerbate spreading of bacteria and formation of necrotic granulomas.[11] However, despite the consensus that AMs are the first innate cells that interact with *Mtb*, not much is known about how AMs participate to mediate control of *Mtb* infection. In the current study, we show that AMs are amongst the earliest infected cells upon exposure to W-Beijing *Mtb* HN878, they accumulate in the airways and express CCR2. During disease progression, we demonstrate that AMs exit the airways and localize within the TB granulomas. Importantly, following *Mtb* HN878 infection, sorted non-airway AMs highly express genes belonging to classical macrophage activation, when compared to airway AMs that

[1]Department of Molecular Microbiology, Washington University School of Medicine in St. Louis, St. Louis, MO 63110, USA; [2]Department of Pathology and Immunology, Washington University School of Medicine in St. Louis, St. Louis, MO 63110, USA; [3]University of Rochester Medical Center, Rochester, NY 14642, USA; [4]Department of Medicine, Washington University School of Medicine in St. Louis, St. Louis, MO 63110, USA; [5]Division of Bacteriology and Parasitology, Tulane National Primate Research Center, Covington, LA 70118, USA and [6]Public Health Research Institute, Rutgers New Jersey Medical School, Newark, NJ 07103, USA
Correspondence: Shabaana A. Khader (khader@wustl.edu)

Received: 6 December 2017 Revised: 26 June 2018 Accepted: 10 July 2018
Published online: 16 August 2018

express a unique transcriptional signature. Depletion of CCR2-expressing cells, specifically at the timing of CCL2 induction and AM egress from the airways, resulted in increased susceptibility to *Mtb* infection, with the accumulation of neutrophils and loss of *Mtb* control. Additionally, we provide new evidence that mutant HN878 lacking PGL expression still resulted in increased susceptibility in CCR2$^{-/-}$ mice. Together, our data provide novel evidence for a protective role for CCR2 in mediating AM localization and immunity against emerging *Mtb* infections.

RESULTS

CCR2 is required for AM accumulation and protective granuloma formation following infection with emerging W-Beijing *Mtb*

Published studies thus far have shown a redundant role for CCR2 in *Mtb* infection, specifically using Euro-American lineage strains such as H37Rv and Erdman.[2,3] These studies have documented either negligible[2] or small[12] increases in *Mtb* burden in CCR2$^{-/-}$ mice, unless CCR2$^{-/-}$ mice were infected with high doses of *Mtb* administered intravenously.[13] Our data confirms these findings as CCR2$^{-/-}$ mice showed similar lung *Mtb* burden when compared with C57BL/6J (B6) mice following infection with *Mtb* H37Rv (H37Rv) (Fig. 1a). Additionally, CCR2$^{-/-}$ mice only showed a small increase in lung burden when infected with another Euro-American clinical *Mtb* strain, CDC1551 (Fig. 1b). Infection with neither H37Rv nor CDC1551 resulted in increased dissemination to the spleen in CCR2$^{-/-}$ infected mice (Fig. 1a, b). In addition, infection with an Indo-Oceanic lineage clinical *Mtb* strain, T17x,[14] also resulted in a small increase in lung and spleen *Mtb* burden in CCR2$^{-/-}$ mice, when compared to B6 infected mice (Fig. 1c). In sharp contrast, when infected with lineage 2 *Mtb* HN878 (HN878), CCR2$^{-/-}$ mice showed significantly increased *Mtb* burden at early days post infection (dpi) which was also maintained during chronic infection (Fig. 1d). Indeed, CCR2$^{-/-}$ HN878-infected mice also exhibited increased dissemination to the spleen, when compared to HN878-infected B6 mice (Fig. 1d). Severe susceptibility with increased lung and spleen *Mtb* burden was also observed when CCR2$^{-/-}$ mice were infected with a pyrazinamide-resistant lineage 2 *Mtb* clinical strain, HN563 (Fig. 1e). These results together show a previously undocumented susceptibility of CCR2$^{-/-}$ mice to *Mtb* infection, projecting a protective role for CCR2 in virulent, emerging W-Beijing *Mtb* infections.

To delineate the cellular mechanisms by which CCR2 mediates protective immunity against HN878 infection, we determined myeloid cell recruitment to the lungs of infected B6 and CCR2$^{-/-}$ *Mtb*-infected mice (Supplementary Fig. 1—gating strategy by flow cytometry). Following H37Rv infection, we observed a trend towards decreased accumulation of monocytes, AMs, recruited macrophages (RMs), mDCs, and neutrophils in the lungs of CCR2$^{-/-}$ H37Rv-infected mice when compared to B6 H37Rv-infected mice (Supplementary Fig. 2a–e) confirming previous findings.[2,13,15] CCR2$^{-/-}$ mice also exhibited lower numbers of RMs, mDCs, and monocytes in the uninfected lungs (Fig. 1f, day 0). Upon infection with HN878, CCR2$^{-/-}$ mice showed significantly decreased early AM and RM accumulation and maintained a small reduction in monocyte accumulation, when compared with B6 HN878-infected lungs (Fig. 1f). Although mDC numbers were lower in uninfected lungs of CCR2$^{-/-}$ mice, there were no significant changes in mDC numbers in CCR2$^{-/-}$ HN878-infected mice when compared to B6 HN878-infected mice (Fig. 1f). Also, the accumulation of activated lung IFN-γ-producing CD4^{+} T cells was comparable between B6 and CCR2$^{-/-}$ mice infected with either H37Rv or HN878 (Supplementary Fig. 2f–h). These results demonstrate that early macrophage accumulation and protective immunity are dependent on CCR2 expression during HN878 infection, but that this requirement is dispensable for H37Rv infection.

The decreased early accumulation of macrophage populations in CCR2$^{-/-}$ HN878-infected mice coincided with significantly increased early accumulation of neutrophils, which was maintained during chronic infection (Fig. 1f). Incidentally, neutrophil accumulation is associated with failed immunity to *Mtb* infection and neutrophils are the predominant infected myeloid cell type.[16–19] In support of this, we observed increased fibrosis and formation of necrotic granulomas in lungs of HN878-infected CCR2$^{-/-}$ mice, when compared with lungs of B6 HN878-infected mice (Fig. 1g, h). Expression of mRNA for tissue remodeling markers such as Arginase-1 (*Arg1*), transforming growth factor (*Tgfb1*), and tumor necrosis factor alpha (*Tnfa*) were also increased in CCR2$^{-/-}$ HN878-infected lungs (Fig. 1i). Additionally, fewer granulomas were found in CCR2$^{-/-}$ *Mtb* HN878-infected lungs, when compared with well-formed granulomas present in B6 HN878-infected lungs (Fig. 1j, k). Finally, although there was decreased accumulation of AMs in CCR2$^{-/-}$ *Mtb*-infected lungs (Fig. 1f), more CD11c^{+} macrophages were infected with *Mtb* within granulomas of CCR2$^{-/-}$ mice, when compared to the AMs in granulomas from B6 mice (Fig. 1l). Together, these data imply that the CCR2 axis is required for formation of protective granulomas during TB. In the absence of CCR2, there are fewer macrophages and fewer protective granulomas formed, instead resulting in an influx of neutrophils and development of necrotic granulomas that do not effectively control *Mtb,* thus leading to increased susceptibility.

AMs are preferentially infected with *Mtb* HN878 and require lung epithelial signaling for accumulation upon infection

To delineate the unique requirement for CCR2 expression during HN878 infection, we used H37Rv-GFP and HN878-GFP *Mtb* reporter strains and addressed if they similarly infect myeloid cell populations, and if *Mtb* infection modulated CCR2 expression on myeloid cells. Following in vivo infection with *Mtb*-GFP reporter strains, AMs more significantly uptake HN878 than H37Rv, suggesting a preferential localization of *Mtb* HN878 within AMs (Fig. 2a, b). Several lung myeloid subsets expressed CCR2 in H37Rv- and HN878-infected mice, including AMs and RMs, monocytes, neutrophils, and mDCs (Fig. 2c–e). Overall, significantly higher numbers of AMs, monocytes, and neutrophils expressing CCR2 were found in the lungs of HN878-infected mice, when compared to H37Rv-infected mice and uninfected mice (Fig. 2c–e). Following H37Rv infection, the RM population predominantly expressed CCR2 when compared to expression levels in uninfected mice (Fig. 2d). In contrast, during HN878 infection, the predominant myeloid cell type expressing CCR2 was the AM population (Fig. 2d). Furthermore, we observed significantly increased CCR2 expression on AMs on a per cell basis during HN878 infection, when compared with AMs during H37Rv infection (Fig. 2f). Thus, our data suggest that AMs preferentially uptake HN878 and specifically upregulate the expression of CCR2.

To further elucidate the *Mtb* strain-specific requirement for the CCR2 axis, we next determined the expression of CCR2 ligands in H37Rv- and HN878-infected lungs. Early expression of mRNA for *Ccl2*, *Ccl7*, and *Ccl12* was significantly higher in HN878-infected lungs, when compared to levels in H37Rv-infected lungs (Fig. 3a). Additionally, CCL2$^{-/-}$ mice infected with *Mtb* HN878 exhibited increased *Mtb* bacterial burden (Supplementary Fig. 3a). However, since CCL2$^{-/-}$ mice did not fully reflect the heightened susceptibility of the CCR2$^{-/-}$ mice to HN878 infection, other ligands such as CCL7 and CCL12 may mediate CCR2 driven protection during *Mtb* HN878 infection. Given the relevance of CCL2 in human disease,[5,20] we chose to focus on CCL2 production in subsequent experiments. To determine the main cellular sources of CCL2 upon infection, we assessed CCL2 levels in supernatants of lung epithelial cells, DCs, and macrophages after in vitro infection with either H37Rv or HN878. We observed that CCL2 production was significantly higher upon infection with HN878 in epithelial cells and DCs (Fig. 3b). In contrast, in macrophages as previously shown,[6] HN878 infection resulted in

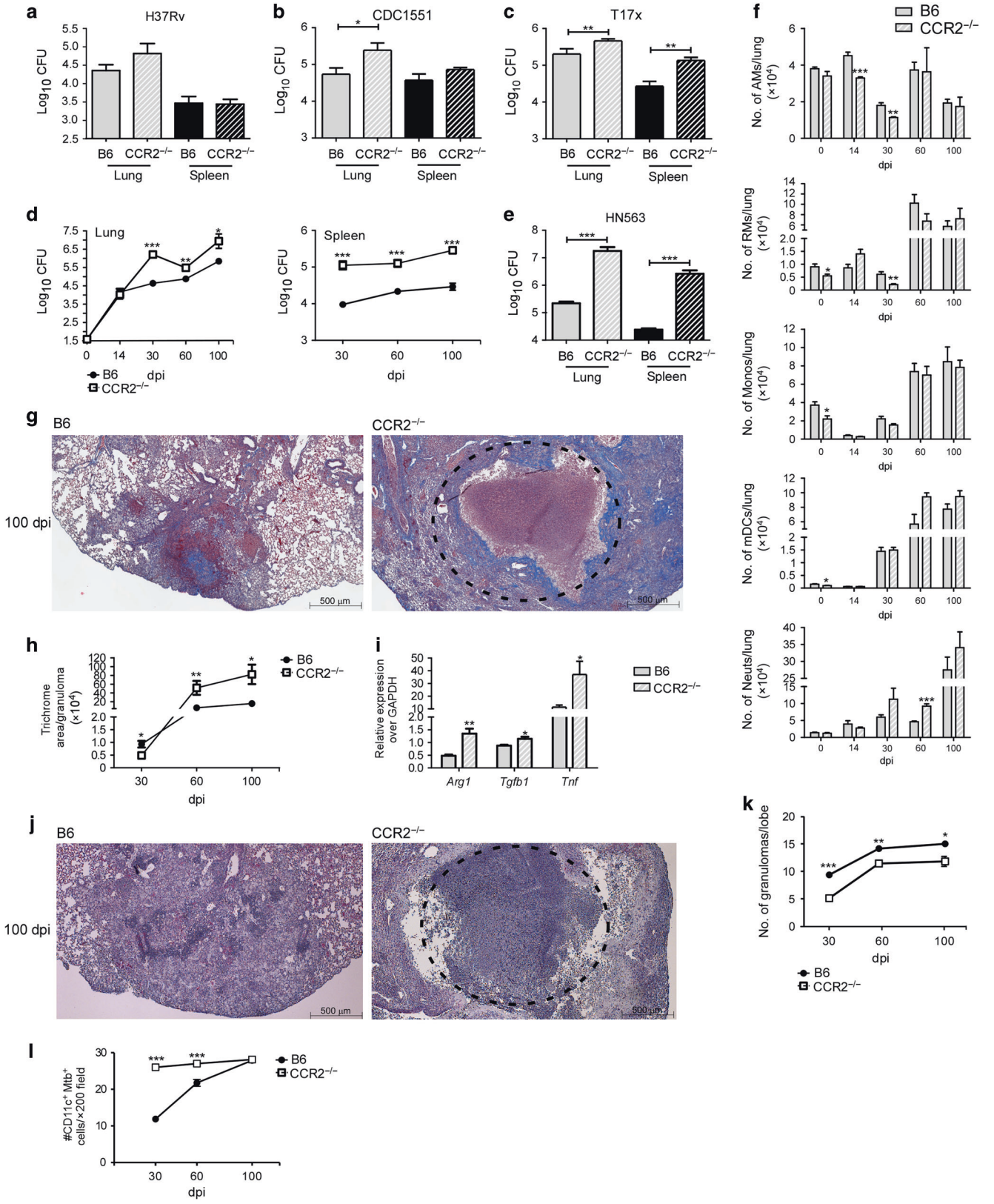

decreased CCL2 production when compared to H37Rv infection (Fig. 3b).

Epithelial cells induced CCL2 in response to infection with HN878, thus we hypothesized that epithelial cell signaling may be involved in chemokine induction and coordinate the localization or myeloid cells, including AMs to form granulomas. Thus, we utilized the IKK2$^{fl/fl}$ Sftpc-Cre mice,[21] which lack canonical IKK and NF-κB signaling in Sftpc-expressing cells, mainly lung epithelial cells.[22] Upon infection of IKK2$^{fl/fl}$ Sftpc-Cre mice with *Mtb* HN878, we observed decreased AM (Fig. 3c) and neutrophil (Fig. 3d)

Fig. 1 CCR2$^{-/-}$ mice show increased susceptibility to low dose aerosol HN878 infection. B6 and CCR2$^{-/-}$ mice were aerosol-infected with ~100 CFU of **a** H37Rv, **b** CDC1551, **c** T17x, **d** HN878, or **e** HN563. Bacterial burden in the lung and spleen was determined by plating **a**–**c**, **e** at 30 dpi or **d** at different dpi. **f** Lung myeloid cell populations were enumerated in B6 and CCR2$^{-/-}$ HN878-infected mice using flow cytometry at indicated dpi. **g**–**k** Pulmonary histology was assessed on FFPE lung sections from 30, 60, and 100 dpi samples stained with **g** Trichrome staining or **j** H&E staining. **h** Inflammatory area expressing collagen was quantified using Visiomorph image processing software to determine lung fibrosis. **i** RNA was extracted from B6 and CCR2$^{-/-}$ HN878-infected lungs and relative mRNA expression of specific genes was determined by qRT-PCR. *Gapdh* was used as internal control. **k** Inflammation was quantified using the morphometric tool of the Zeiss Axioplan microscope to determine the total number of granulomas per lobe. **l** The total number of CD11c^{+} *Mtb* containing cells per 200× was determined by counting in FFPE lung sections of B6 and CCR2$^{-/-}$ mice. AMs alveolar macrophages, RMs recruited macrophages, Monos monocytes, mDCs myeloid dendritic cells, Neuts neutrophils. $n = 5$, **a**–**e** Student's *t*-test between B6 and CCR2$^{-/-}$, **f** 2-way ANOVA with Bonferroni's post test. **h**–**l** Student's *t*-test was used to determine differences per time point

accumulation in HN878-infected lungs, without any changes in RM accumulation (Fig. 3e) when compared to myeloid cell accumulation in infected littermate controls. Associated with decreased AM accumulation, IKK2$^{fl/fl}$ Sftpc-Cre HN878-infected mice were more susceptible and exhibited increased lung *Mtb* CFU at 30 dpi (Fig. 3f). We found that total protein levels of C–C-chemokines such as CCL2 and CCL3, and CXC-chemokines such as CXCL2 were not different in lung homogenates of IKK2$^{fl/fl}$ Sftpc-Cre mice, compared to littermate controls (Supplementary Fig. 3b). However, we specifically found that lungs of IKK2$^{fl/fl}$ Sftpc-Cre mice exhibited fewer E-cadherin expressing epithelial cells producing CCL2 protein, when compared to littermate controls (Fig. 3g). The protein levels of CXCL1, a neutrophil-attracting chemokine, were reduced in total lung homogenates of IKK2$^{fl/fl}$ Sftpc-Cre mice (Supplementary Fig. 3b), likely resulting in the decreased neutrophil recruitment observed in infected mice (Fig. 3d). These findings suggest that early epithelial signaling has a role in coordinating the accumulation of myeloid cells, specifically AMs and neutrophils, to the lungs during infection.

CCR2 expression mediates AMs to egress from airways and localizes within TB granulomas

CCL2 is produced by HN878-infected epithelial cells and DCs, and thus we next examined if the CCR2 axis was involved in AM movement out of the airways. To address this, we specifically labeled myeloid cells within the airways by delivering fluorophore-conjugated CD45.2 antibody intratracheally (IT) to *Mtb* HN878-infected mice prior to harvest (Supplementary Fig. 4a–d). This technique allowed us to distinguish between broncho-alveolar lavage (BAL) stain positive airway CCR2^{+} AMs (CD45.2^{+}CCR2^{+}CD11c^{+}SiglecF^{+}) and BAL stain negative non-airway CCR2^{+} AMs that are not exposed to the CD45.2 antibody (CD45.2^{-}CCR2^{+}CD11c^{+}SiglecF^{+}) (Fig. 4a). To validate the technique, we demonstrated that delivery of CD45.2 antibody into the airways does not leak into the interstitium in naïve mice (Supplementary Fig. 4d). However, when lung injury is induced in mice by intratracheal instillation of HCl, we observed increased dispersion of CD45 antibody into the interstitium (Supplementary Fig. 4d). Additionally, mice undergoing lung injury due to treatment with HCl showed increased frequency of total lung cells and myeloid cells stained with CD45.2 antibody when compared with CD45.2^{+} lung cells in naïve PBS-treated mice (Supplementary Fig. 4a–c). Furthermore, when BAL was collected immediately after delivery of CD45.2 antibody IT, we found that the airway-localized AMs were ~99% CD45.2^{+} in both uninfected and *Mtb*-infected mice (Supplementary Fig. 4e, left panel), though AMs were a smaller proportion of the total airway cells during infection (Supplementary Fig. 4e, right panel).

During *Mtb* infection, we observed an overall increase in AM accumulation in the lung (Fig. 4b). In addition, we found that early during infection, of the airway labeled myeloid cells, AMs were the most represented cell type, followed by DCs (Fig. 4c). However, as infection progressed, neutrophils along with monocytes were increasingly represented in the airway, while AMs were less represented (Fig. 4c). We observed increased CCR2^{+} AM accumulation early following infection, especially within the airways (Fig. 4d). As infection progressed, we observed decreased CD45.2^{+}CCR2^{+} AMs localizing within the airways and increased non-airway CD45.2^{-}CCR2^{+} AMs, suggesting either an egress of bonafide AMs from the airway, or the presence of recruited, monocyte-derived, AM-like cells within the tissue (Fig. 4d). The timing of these changes in localization coincided with the timing of increased CCR2 ligand expression in the lung at 21 dpi (Fig. 3a).

To determine the identity and functional relevance of the AM populations, we sorted for highly purified airway AMs (~99% purity, Supplementary Fig. 5a) (CD45.2^{+}CD11c^{+}SiglecF^{+}) from uninfected and infected mice, and non-airway AMs from infected mice (~95% purity, Supplementary Fig. 5a) (CD45.2^{-}CD11c^{+}SiglecF^{+}) and carried out RNA sequencing. We confirmed that both populations were in fact bonafide AMs by examining the common AM gene signature[23,24] between groups (i.e., *Siglecf*, *Pparg*, *Tgfbr2*, *Csf2r, Mertk, Itgax, Lyz2*, and *Fcgr1*). We also confirmed that the AM populations did not highly express genes associated with monocyte-derived interstitial or RMs[25] (*Ly6c1, Itgam*, and *CD163*) (Supplementary Table 1, 2a-b). These data support our hypothesis that both airway and non-airway AMs are not interstitial monocyte-derived macrophages[25] but in fact bonafide AM populations.

According to the RNA-Seq analysis, non-airway AMs expressed significantly higher mRNA levels (according to DESeq2[26]) for genes belonging to classical macrophage activation including inducible nitric oxide synthase (*Nos2*), CD40 antigen (*Cd40*), S100 calcium binding protein A8 (*S100a8*), Guanylate binding protein 2 (*Gbp2*), Lysozyme 1 (*Lyz1*), and Lipocalin (*Lcn2*), when compared with sorted airway AMs (Fig. 4e and Supplementary Table 3). Additionally, non-airway AMs also expressed significantly higher mRNA for genes such as Matrix metallopeptidases (*Mmp2*, *Mmp14*) and proinflammatory chemokines such as *Cxcl9*, *Cxcl16*. In addition, mRNA belonging to classical macrophage transcriptional signatures such as Basic leucine zipper transcription factor, ATF-like 2 (*Batf2*),[27] and Interferon regulatory factor 8 (*Irf8*),[28] were significantly higher in sorted non-airway AMs than airway AMs. Transcriptional profiles of non-airway AMs when compared with airway AMs showed significantly higher expression of pathways associated with infections, complement cascade, and the phagosome activation (Supplementary Table 4).

Alternatively, only 12 genes were significantly expressed at higher levels in airway AMs during infection, when compared with non-airway AMs isolated from *Mtb*-infected mice (Fig. 4e and Supplementary Table 5), including inhibitor of DNA binding 1 (*Id1;* expressed by tissue-resident macrophages[29]) and growth differentiation factor-15 (*Gdf15*), which has been reported to drive expression of CCR2 in macrophages.[30] Further, significantly higher gene expression in airway AMs was observed for Toll-like receptor (TLR)-induced inflammatory responses such as Polo-like kinase 3 (*Plk3*)[31] and Pleckstrin homology like domain, family A, member 1 (*Phlda1*),[32] and the cholesterol-trafficking START domain containing 9 (*Stard9*) genes. Genes significantly higher in airway AMs from infected mice compared to uninfected mice demonstrated significant enrichment for pathways associated with metabolic

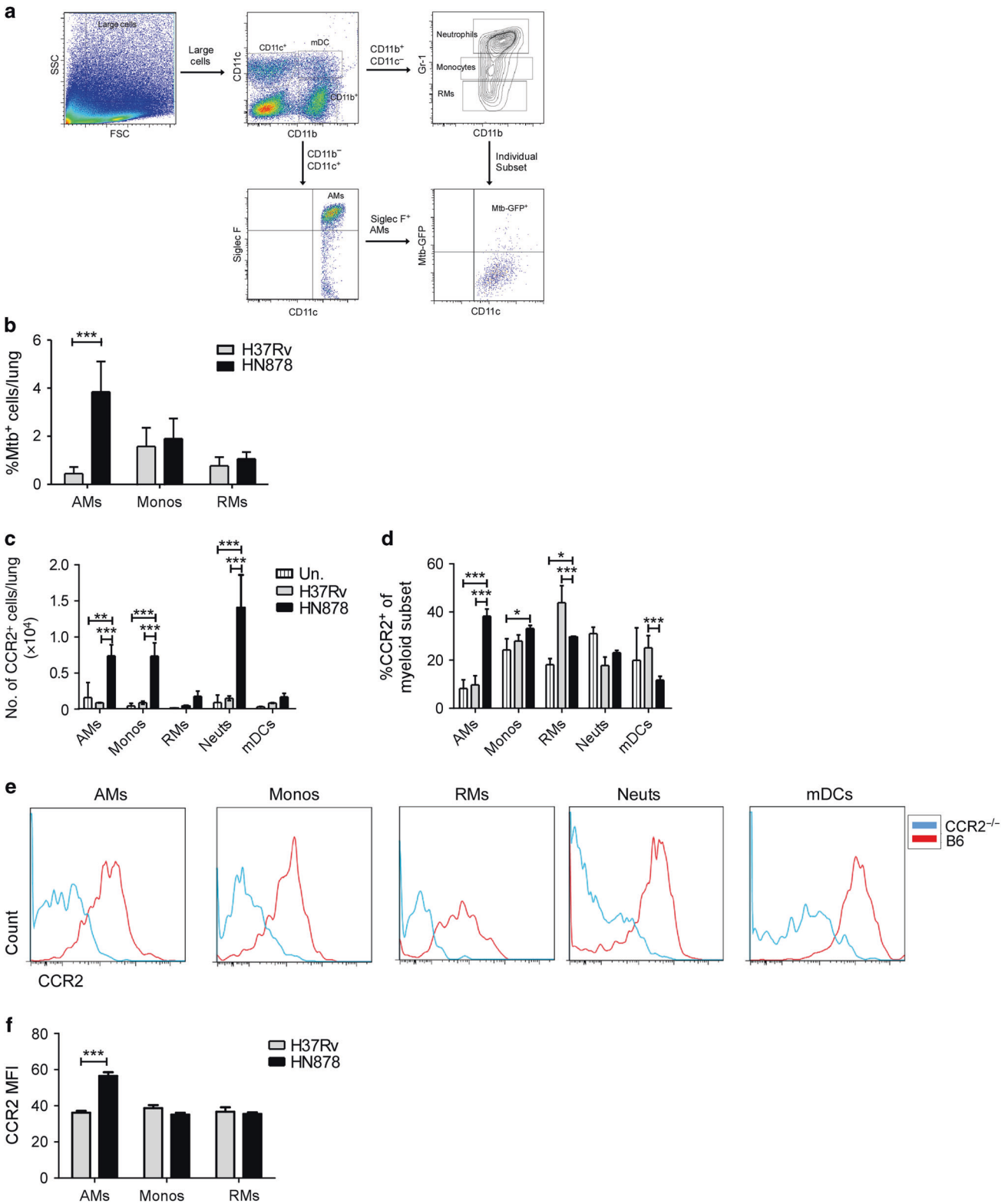

pathways, antigen processing and phagocytosis (Supplementary Table 6). In addition, genes associated with several key signaling pathways associated with cytoskeletal rearrangement and diapedesis were downregulated during infection in airway AMs (Supplementary Table 7). Together, our results indicate that airways AMs during infection upregulate a unique transcriptional signature associated with phagocytosis and antigen-presentation, when compared to non-airway AMs, who are more classically activated for intracellular killing and T cell activation.

To mechanistically examine the ability of CCR2^{+} AMs to egress from the airways and localize within the TB granulomas during HN878 infection, we used an adoptive transfer model with CCR2-GFP-expressing AMs. We purified CD11c^{+} lung cells (Supplementary Fig. 5b) from HN878-infected CCR2-GFP($^{+}$/KI)

Fig. 2 AMs are preferentially infected with HN878 and CCR2 expression on AMs is *Mtb* strain-dependent. **a** The flow cytometry gating strategy for myeloid populations. Briefly, AMs were defined as $CD11b^{-}CD11c^{+}SiglecF^{+}$ cells. mDCs were defined as $CD11b^{+}CD11c^{+}$ cells. Neutrophils were defined as $CD11b^{+}CD11c^{-}Gr\text{-}1^{hi}$ cells, monocytes were defined as $CD11b^{+}CD11c^{-}Gr\text{-}1^{lo}$ cells, and recruited macrophages were defined as $CD11b^{+}CD11c^{-}Gr\text{-}1^{-}$ cells. *Mtb*-GFP^{+} cells were gated from individual subsets. **b** B6 mice were aerosol-infected with ~100 CFU of H37Rv-GFP or HN878-GFP and myeloid cell subsets infected with *Mtb*-GFP were determined by flow cytometry on 30 dpi ($n = 5$). **c**, **d** B6 mice ($n = 5$) were infected with aerosolized H37Rv or HN878 and the total number (**c**) and percentage (**d**) of $CCR2^{+}$ myeloid lung cell populations were determined by flow cytometry and compared to uninfected controls. **e** Representative histograms of each subset displaying CCR2 expression by antibody staining compared to $CCR2^{-/-}$. **f** Mean fluorescence intensity (MFI) of CCR2 expression on myeloid populations was normalized relative to MFI of unstained, uninfected controls. Un. uninfected, AMs alveolar macrophages, Monos monocytes, RMs recruited macrophages, Neuts neutrophils, mDCs myeloid dendritic cells. **a**–**d** 2-Way ANOVA with Bonferroni post test was used. **f** Student's *t*-test

mice[33] or CCR2-GFP(KI/KI) mice. CCR2-GFP($^{+}$/KI) mice have one functional allele for CCR2, but also express GFP, while CCR2-GFP (KI/KI) mice have both nonfunctional, GFP^{+} alleles. We adoptively transferred the $CD11c^{+}$ cells into the airways of HN878-infected B6 mice, and using SiglecF to further identify AMs, $CD11c^{+}$ $SiglecF^{+}$ CCR2-GFP^{+} AMs were tracked within TB granulomas (Fig. 5a). We observed that $CD11c^{+}$ $SiglecF^{+}$ CCR2-GFP($^{+}$/KI) AMs adoptively transferred into the airways localized within the TB granulomas (Fig. 5b). In contrast, adoptive transfer of CCR2-GFP (KI/KI) AMs into the airways resulted in notably reduced accumulation within the TB granulomas (Fig. 5c). Furthermore, we observed increased migration of *Mtb*-stimulated CCR2-GFP ($^{+}$/KI) macrophages in response to HN878-infected but not H37Rv-infected epithelial cell supernatant. However, *Mtb*-stimulated CCR2-GFP(KI/KI) macrophages did not migrate in response to *Mtb*-infected epithelial cell supernatants, suggesting that the macrophage migration in response to infection is CCR2-dependent (Fig. 5d). Furthermore, localization of *Ccl2* mRNA is within TB granulomas in HN878-infected B6 lungs, while *Ccl2* mRNA expression was localized outside of cavitary TB granulomas in $CCR2^{-/-}$ HN878-infected lungs (Fig. 5e). Additionally, a higher percentage of AMs were found in the airways of $CCR2^{-/-}$ HN878-infected lungs when compared to B6 HN878-infected mice (Fig. 5f). These data suggest that CCR2 plays a role in AM localization within the TB granuloma, and that without a functional CCR2, AMs less efficiently migrate from the airways to localize within the TB granulomas.

CCR2 expression at the time of airway AM egress is critical for control of *Mtb* HN878 infection

CCR2-DTR mice have diphtheria toxin receptor (DTR) inserted between the first and second codon of CCR2,[34] and treatment of CCR2-DTR mice with diphtheria toxin (Dtx) resulted in depletion of all CCR2-expressing cells. Previously, depletion of CCR2-expressing cells following *Mtb* Erdman infection reduced monocyte and monocyte-derived populations, but did not result in increased *Mtb* susceptibility.[3] To address the timing of the CCR2 requirement for protection following HN878 infection, we similarly used CCR2-DTR mice.[3] CCR2-DTR mice were infected with HN878, and CCR2-expressing cells were depleted either early at the time of infection (−1 to 5 dpi) or later at the time of AM egress from the airways (12–18 dpi) (Fig. 4d). Transient depletion of all CCR2-expressing cells around 12–18 dpi but not at the time of infection resulted in a significant increase in *Mtb* burden (Fig. 6a–d). Depletion of CCR2-expressing cells at 12–18 dpi also resulted in increased accumulation of neutrophils, monocytes, and RMs in the lung and sharply decreased number of AMs, when compared to PBS-treated *Mtb*-infected mice (Fig. 6b). Additionally, CCR2-DTR that received Dtx between 12 and 18 dpi also showed increased inflammation, when compared to control CCR2-DTR mice that received PBS (Fig. 6c). In contrast, CCR2-DTR mice that received Dtx around the time of infection did not show any differences in AM numbers, but showed decreased accumulation of neutrophils, monocytes and RMs and coincident decreased inflammation (Fig. 6e, f). Together, these results demonstrate that transient depletion of CCR2-expressing cells coincident with the time of AM egress from the airways resulted in decreased AM accumulation and increased susceptibility to HN878 infection. In contrast, depletion of CCR2-expressing cells around the time of infection, while dampening RM and monocyte accumulation, did not impact AM accumulation and only minimally increased *Mtb* control.

To further confirm the role of $CCR2^{+}$ AMs in protection against HN878 *Mtb* infection, we delivered B6 macrophages stimulated in vitro with irradiated *Mtb* into the airways of $CCR2^{-/-}$ HN878-infected mice. Adoptive transfer of B6 macrophages rescued the increased susceptibility observed in $CCR2^{-/-}$ *Mtb*-infected mice, yielding decreased lung bacterial burden equivalent to B6 *Mtb*-infected mice (Fig. 6g). These data suggest that the susceptibility associated with $CCR2^{-/-}$ mice coincides with lack of macrophage accumulation in the lung, and that adoptive transfer of B6 macrophages into airways is sufficient to reverse susceptibility *Mtb* in $CCR2^{-/-}$ *Mtb*-infected mice.

Dependence on CCR2 for protective immunity to *Mtb* HN878 is not driven solely by PGL expression

Recently, *M. marinum* expressing PGL has been shown to be involved in the induction of CCL2 and recruitment of CCR2-expressing permissive macrophages in zebrafish mycobacterial infection model.[8,9] Thus, we next addressed if the absence of PGL in *Mtb* HN878 would result in lack of a role for CCR2 in controlling *Mtb* HN878 infection in mice. Thus, B6 and $CCR2^{-/-}$ mice were infected with a recombinant *Mtb* HN878 mutant harboring a mutation within *pks1-15* (HN878 *pks1-15::hygB*) rendering *Mtb* PGL deficient.[6] Upon infection with *Mtb* HN878 *pks1-15::hygB*, $CCR2^{-/-}$ mice were still more susceptible to infection when compared with B6 infected mice (Fig. 7a). This coincided with decreased accumulation of AMs, RMs, and monocytes, increased neutrophil accumulation (Fig. 7b), and severe pulmonary disease (Fig. 7c) in $CCR2^{-/-}$ infected mice when compared with B6 infected mice. Additionally, while in vitro infection of macrophages and DCs with HN878 *pks1-15::hygB* resulted in decreased CCL2 when compared to HN878 infection[6] (Fig. 7d), comparable induction of CCL2 was observed upon infection of lung epithelial cells with HN878 and HN878 *pks1-15::hygB* (Fig. 7e). These data are also supported by localized expression of *Ccl2* mRNA within TB granulomas in lungs of B6 and $CCR2^{-/-}$ mice infected with HN878 *pks1-15::hygB* (Fig. 7f). These data suggest that PGL expression is not the only key determinant for a protective role for CCR2 in *Mtb* HN878 infection, as *Mtb* H37Rv and HN878 also differ in expression of several other key components in their cell walls.[35]

DISCUSSION

In humans, polymorphisms in CCL2 have been associated with pulmonary TB,[5] while mouse infection studies have shown that CCR2 expression is dispensable for protective immunity to infection with aerosolized Euro-American lineage 4 *Mtb* strains.[2] Zebrafish modeling of granulomas using *M. marinum* has proposed that the CCR2–CCL2 axis through interactions with virulence factors drives the generation of permissive

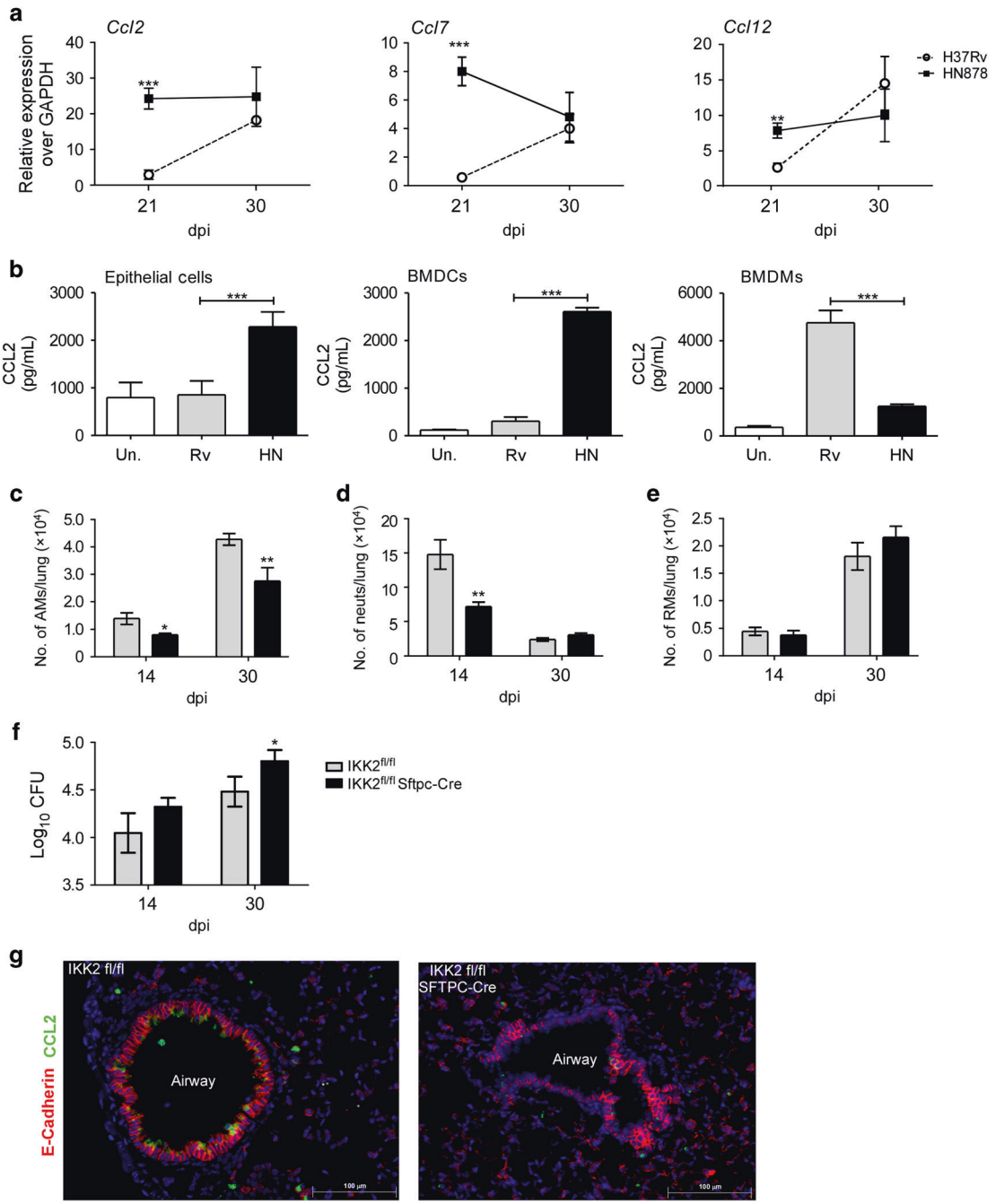

Fig. 3 Increased early CCR2 ligand expression is induced in the lung following HN878 infection. **a** RT-PCR analysis was performed at 21 and 30 dpi to determine mRNA expression for *Ccl2*, *Ccl7*, and *Ccl12* in lungs of H37Rv- or HN878-infected mice ($n = 5$ per group, per time point). **b** C10 epithelia, BMDCs, and BMDMs were cultured and infected with indicated *Mtb* strains at an MOI of 1 for 48 h ($n = 6$). Supernatants were analyzed by multiplex or ELISA assay for CCL2. **c**–**e** IKK2$^{fl/fl}$ Sftpc-Cre mice and littermate controls were infected with HN878 for 14 ($n = 7$) and 30 ($n = 5$) dpi and the accumulation of **c** AMs, **d** neutrophils, and **e** RMs were calculated by flow cytometry. **f** Bacterial burden in the lung was determined by plating at 14 ($n = 7$ per group) and 30 dpi ($n = 5$ per group) in IKK2$^{fl/fl}$ Sftpc-Cre mice and littermate controls. **g** Confocal microscopy of lung sections stained for E-cadherin (red) and CCL2 (green) in IKK2$^{fl/fl}$ Sftpc-Cre mice and littermate controls. AMs alveolar macrophages, Neuts neutrophils, RMs recruited macrophages. **a** 2-Way ANOVA with Bonferroni post test, **b** 1-way ANOVA with Tukey's post test. **c**–**f** Student's *t*-test was used to compare between groups per time point

macrophages and promotes mycobacterial replication and pathogenesis.[8] In the current study, using murine models, we provide novel evidence that the CCR2 axis is critical for protective immunity against infection with emerging *Mtb* lineages, such as the W-Beijing *Mtb* strains. Our data demonstrate that AMs express CCR2 that is required for localization of AMs within the TB granulomas. In the absence of CCR2, AMs fail to localize within TB granulomas, resulting instead in accumulation of neutrophils and development of necrotic TB lesions, a characteristic of failed immunity in TB. Additionally, we show that the requirement for CCR2 for protective immunity to *Mtb* HN878 is not solely dependent on expression of PGL and PGL-mediated modulation of this chemokine axis. Thus, our study provides novel insights by projecting that CCR2 expression,

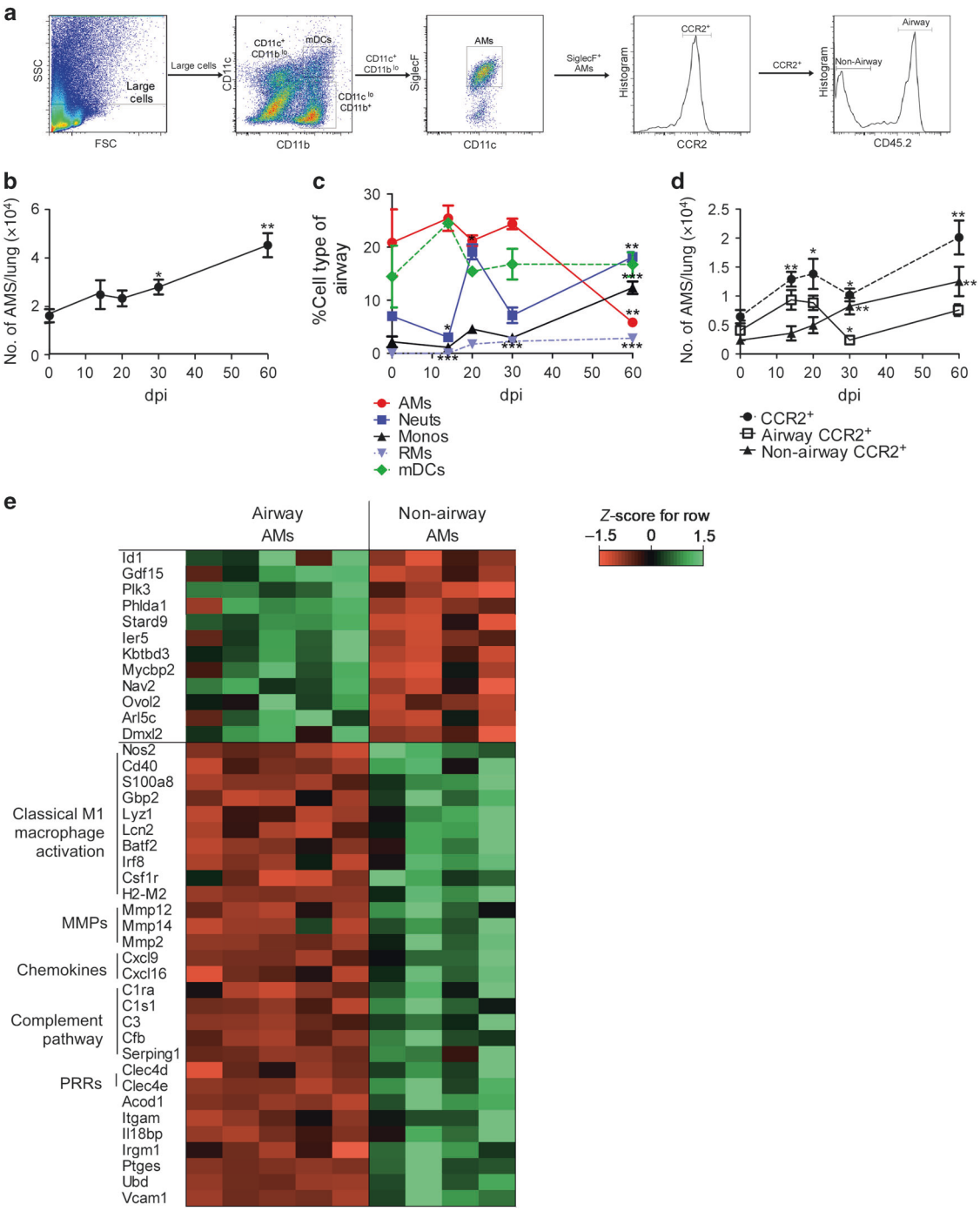

Fig. 4 CCR2 expression is required for AMs to egress from airways and localize within TB granulomas. Single cell lung suspensions from uninfected and infected mice ($n = 5$) were prepared and **a** the gating strategy for airway and non-airway AMs is shown. The percentage and number of specific cell subsets with airway label CD45.2 delivered IT is shown. $CD11c^{+}CD11b^{lo}SiglecF^{+}CD45.2^{+}$ cells were gated as airway AMs, while $CD11c^{+}CD11b^{lo}SiglecF^{+}CD45.2^{-}$ cells were gated as non-airway AMs. **b** The total number of AMs over the time course of HN878 in B6 mice was determined by flow cytometry ($n = 5$ per time point). **c** From total airway labeled cells ($CD45.2^{+}$), the percentage of each myeloid cell type was determined in HN878-infected B6 mice by flow cytometry. **d** Total $CCR2^{+}$ AMs, $CCR2^{+}$ airway ($CD45.2^{+}$) AMs, and $CCR2^{+}$ non-airway ($CD45.2^{-}$) AMs over the course of HN878 infection in B6 mice were determined by flow cytometry. **e** *Z*-score Pearson correlation-based clustering of differentially expressed genes of interest (all 12 significantly differentially expressed genes in airway AMs, and 29 genes of functional interest that were higher in non-airway AMs). AMs alveolar macrophages, Neuts neutrophils, Monos monocytes, RMs recruited macrophages, mDCs myeloid dendritic cells, MMPs matrix metallopeptidases, PRRs pattern recognition receptors. **b**–**d** Each time point was compared to baseline d0 counts using Student's *t*-test. **e** The gene expression levels of a subset of significantly differentially expressed genes between airway and non-airway AMs (according to DESeq)

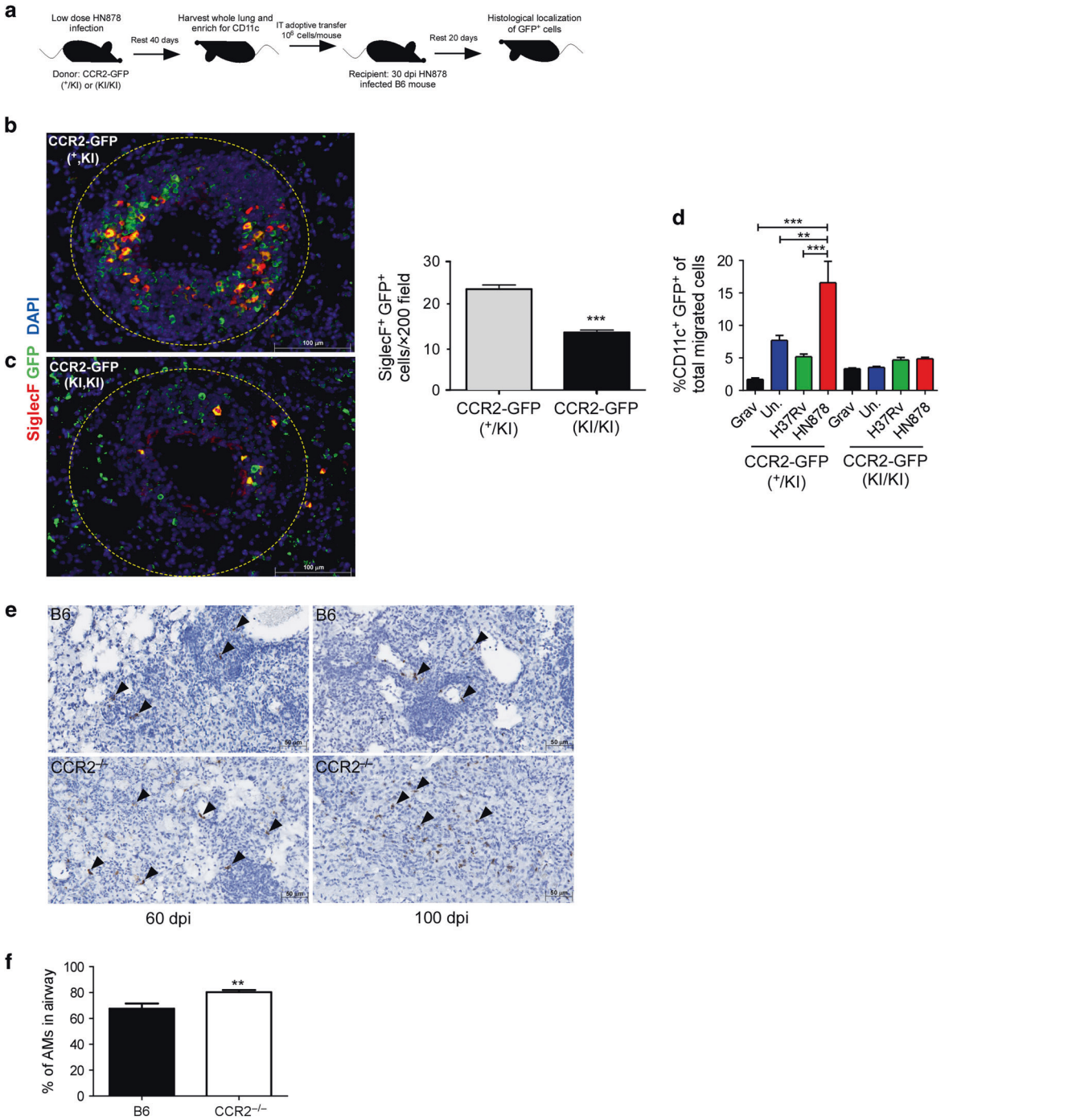

Fig. 5 CCR2 is required for AM localization within TB granulomas. **a** CD11c$^+$ cells were purified from lungs of 30 dpi HN878-infected CCR2-GFP ($^+$/KI) or CCR2-GFP(KI/KI) mice and 10^6 cells were IT transferred into B6 HN878-infected mice ($n = 5$) at 30 dpi. **a**–**c** Lungs were harvested at 50 dpi and examined for localization of SiglecF$^+$ GFP$^+$ cells within TB granulomas using the morphometric tool of the Zeiss Axioplan microscope. **d** CCR2-GFP($^+$/KI) or CCR2-GFP(KI/KI) BMDMs were stimulated in vitro with 20 μg/mL irradiated *Mtb* HN878 for 24 h. Migration towards uninfected, H37Rv- or HN878-infected epithelial cell supernatants was analyzed via transwell chemotaxis assays and flow cytometry ($n = 3$). **e** *Ccl2* mRNA localization was determined within FFPE lung sections from B6 and CCR2$^{-/-}$ HN878-infected using RNAScope in situ hybridization (ISH). Arrows point to *Ccl2* mRNA localization (brown). **f** B6 and CCR2$^{-/-}$ mice ($n = 5$) were infected with HN878 and percentage of AMs with airway label CD45.2 delivered IT was calculated on 14 dpi by flow cytometry. Grav gravity control, Un. uninfected, AMs alveolar macrophages. $n = 5$. **b**, **c** Student's *t*-test. $n = 3$. **d** 2-Way ANOVA with Bonferroni post test. **f** Student's *t*-test

especially on AMs, is required for protective immunity against emerging *Mtb* strains.

AMs are a tissue-resident macrophage lineage that under homeostatic conditions are believed to mature during neonatal development.[36] However, under conditions of inflammation, inflammatory monocytes, perhaps through a transient lung-resident macrophage population may also give rise to AMs.[36] During *Mtb* infection, although it is widely believed that tissue-resident AMs are the primary innate cell type that are infected,[37] the functional relevance of AMs during *Mtb* infection is unclear.

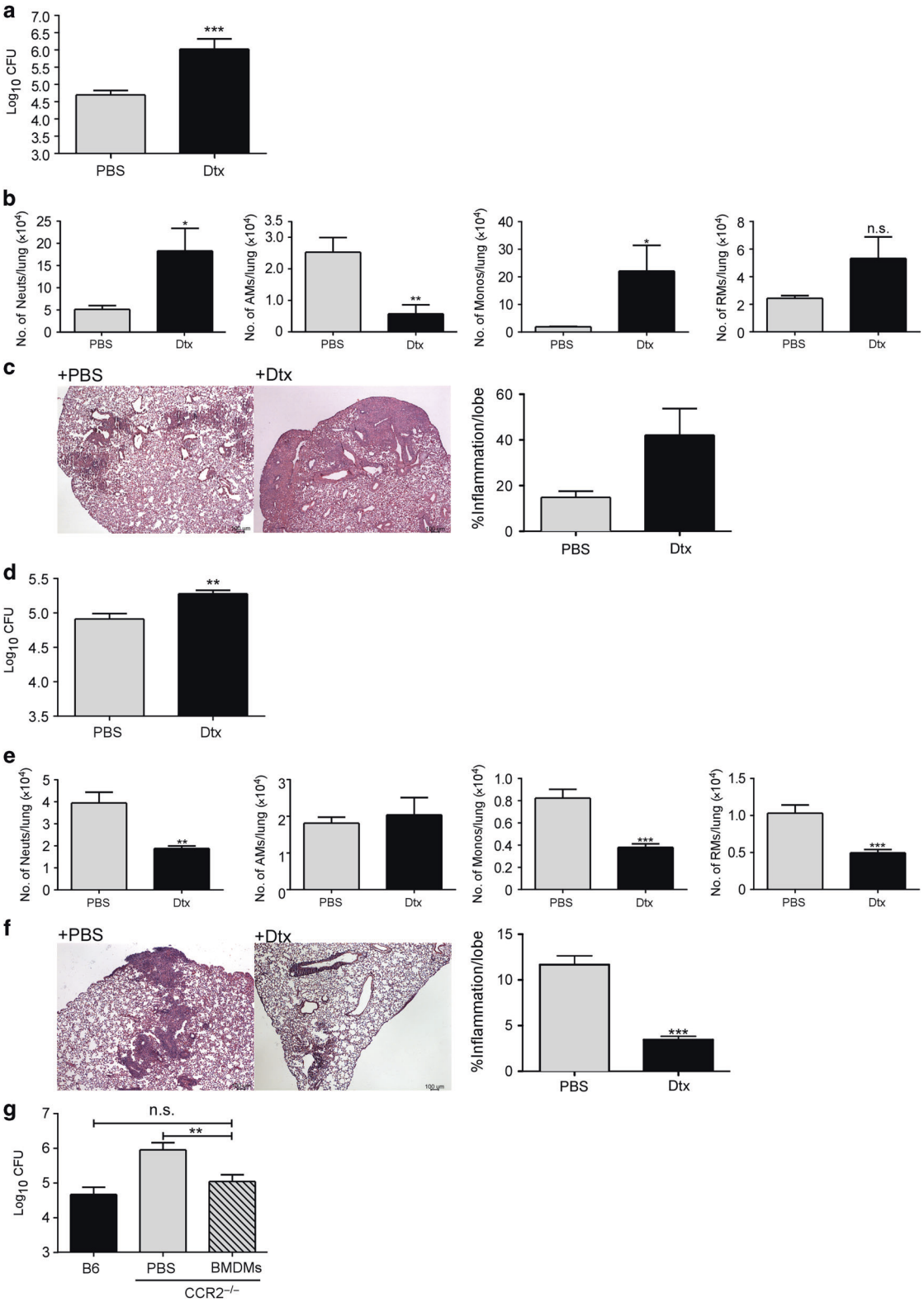

Fig. 6 Depletion of CCR2^{+} cells at the time of AM egress from airways increases susceptibility to HN878 infection. CCR2-DTR mice ($n = 4$) were infected with HN878 and administered Dtx **a**–**c** IP at 12, 14, and 16 dpi or d–f at −1, 1, and 3 dpi. **a**, **d** Lung bacterial burden was determined by plating on 30 dpi. **b**, **e** Neutrophil, AM, monocyte, and RM numbers were determined in PBS-treated and Dtx-treated CCR2-DTR mice at 30 dpi. **c**, **f** Pulmonary histology was assessed on FFPE lung sections stained with H&E, and inflammatory area was quantified using the morphometric tool of the Zeiss Axioplan microscope. **g** B6 ($n = 5$) and CCR2$^{-/-}$ mice ($n = 8$ per group) were infected with HN878, and CCR2$^{-/-}$ mice received either PBS or HN878-stimulated BMDMs delivered IT on 15 and 21 dpi. Lungs were harvested at 30 dpi and bacterial burden was determined by plating. Neuts neutrophils, AMs alveolar macrophages, Monos monocytes, RMs recruited macrophages. **a**–**f** Student's *t*-test. **g** 1-Way ANOVA with Tukey's post test

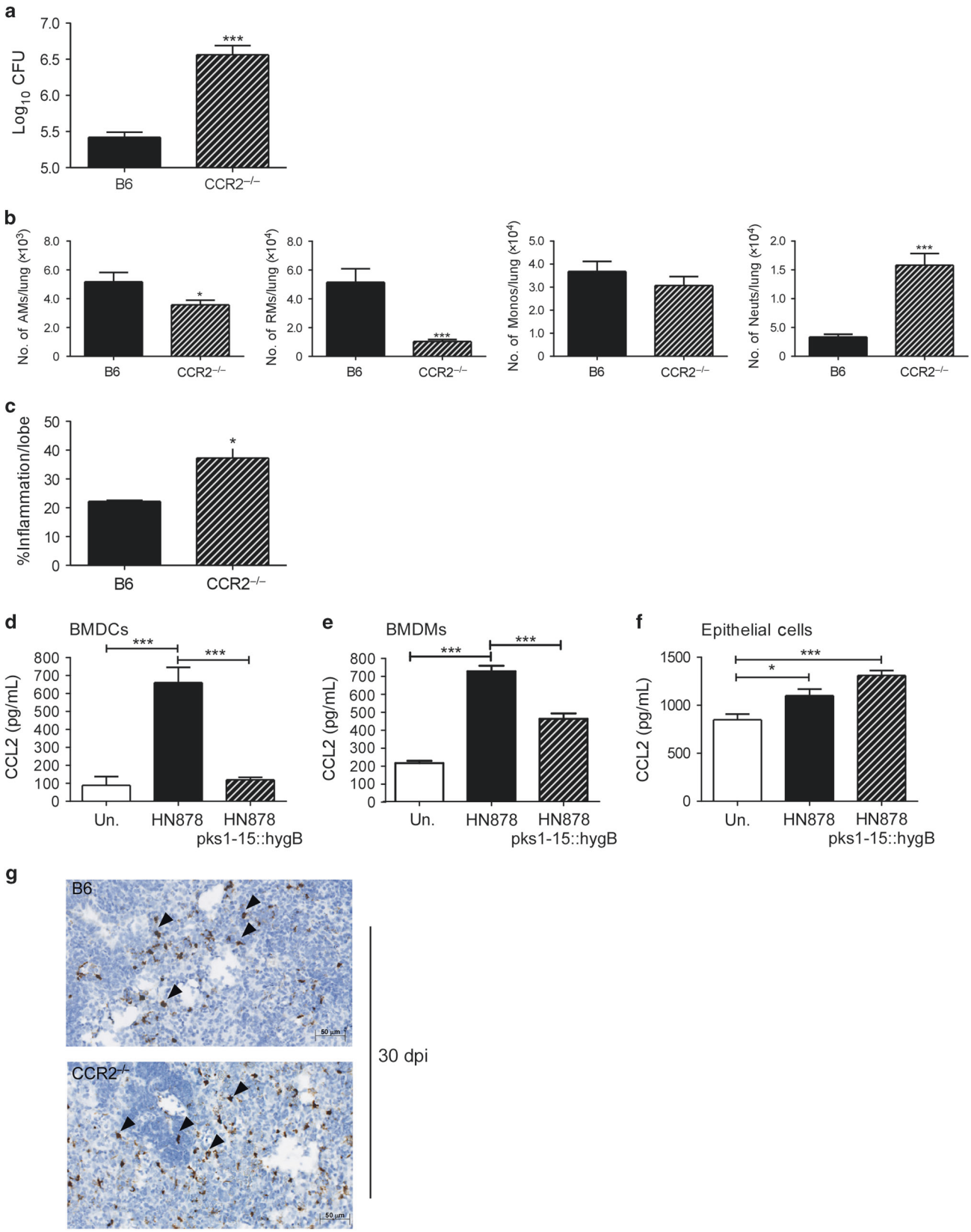

Utilizing the zebrafish granuloma model, it has been shown that *M. marinum* can be transported across neuroepithelial barriers by macrophages and results in CCL2-mediated recruitment of permissive monocyte-derived macrophages that mediate formation of the granuloma to enhance disease pathogenesis.[8,9] Using a murine model, our studies here show that following infection with *Mtb* HN878, bonafide AMs increase in the lung following *Mtb* infection, and they localize within the airway. As

Fig. 7 Dependence on CCR2 for protective immunity to *Mtb* HN878 is not driven by PGL expression. B6 and CCR2$^{-/-}$ mice ($n = 5$) were aerosol-infected with ~100 CFU HN878 *pks1-15::hygB*. **a** Lung bacterial burden was determined by plating on 30 dpi. **b** Lung myeloid cell populations of AMs, RMs, monocytes, and neutrophils were enumerated in B6 and CCR2$^{-/-}$ HN878 *pks1-15::hygB* infected mice using flow cytometry. **c** Pulmonary histology was assessed on FFPE lung sections stained with H&E, and inflammatory area was quantified using the morphometric tool of the Zeiss Axioplan microscope. **d**–**f** BMDCs, BMDMs, and C10 epithelial cells were cultured and infected with indicated *Mtb* strains at an MOI of 1 for 48 h ($n = 5$). Supernatants were analyzed by multiplex or ELISA assay for CCL2. **g** *Ccl2* mRNA localization was determined within FFPE lung sections from B6 and CCR2$^{-/-}$ HN878-infected using RNAScope in situ hybridization (ISH). Arrows point to *Ccl2* mRNA localization (brown). AMs alveolar macrophages, RMs recruited macrophages, Monos monocytes, Neuts neutrophils. **a**–**c** Student's *t*-test. **d**–**f** 1-Way ANOVA with Tukey's post test

infection progresses and TB granulomas form, our results show that AMs respond to CCL2-dependent chemokine signals likely from lung epithelial cells to egress from the airways. Furthermore, adoptive transfer of CD11c^{+} SiglecF^{+} AMs expressing CCR2 localized within granulomas, and AMs not expressing CCR2 did not localize within granulomas, suggesting that AMs may require CCR2 expression to respond to epithelial signals and localize into granulomas. Additionally, we show that HN878 *pks1-15::hygB* infection still results in increased susceptibility in CCR2$^{-/-}$ mice. Thus, the protective versus disease-promoting features of the CCR2 axis and AMs in mycobacterial infections in mouse versus zebrafish model may be due to (1) differences in the animal models used, (2) a specific feature of AM trafficking from airways that are not observed in zebrafish macrophages, or (3) due to the fact that *M. marinum* PGLs contain a monosaccharide while *Mtb* PGL contain a trisaccharide domain.[38]

Ligands for CCR2, namely CCL2, CCL7, and CCL12 are induced in response to *Mtb* infection in mice, non-human primates, and humans.[2,39,40] Despite this, studies in the last decade have shown that CCR2$^{-/-}$ mice display negligible or low susceptibility to low dose aerosolized *Mtb* infection belonging to the Euro-American lineage 4, such as H37Rv and Erdman.[2,12] Our data show that when W-Beijing family lineage 2 clinical *Mtb* strains are used, the absence of CCR2 in the CCR2$^{-/-}$ or deletion of CCR2 in CCR2-DTR mice render mice more susceptible to infection, with coincident defects in macrophage accumulation, instead promoting neutrophil accumulation, an immune cell type associated with failed immunity.[16–19] The influx of neutrophils may be a direct response to the tissue damage and inflammatory environment brought on by the lack of apoptotic clearance and anti-inflammatory signaling of AMs.[41] This increase in susceptibility in CCR2$^{-/-}$ mice is not just limited to lineage 2 but also to clinical isolates within the Euro-American lineage and Indo-Oceanic lineages, albeit not to the same extent as in W-Beijing *Mtb* infection. The observation that infection with the HN878 mutant lacking PGLs still requires CCR2 for AM accumulation and protective immunity supports the idea that expression of other factors by emerging *Mtb* strains are likely involved. It is possible that the observed *Mtb* strain-dependent response is due to distinct cellular responses brought on by pattern recognition and phagocytic receptor interactions with *Mtb* strain-specific membrane lipids and virulence factors.[35] This is supported by published data that *Mtb*-associated membrane lipids and other virulence factors lead to differential transcriptional and metabolic profiles in macrophages.[42–44]

Upon infection with Streptococcus, AMs can leave the airway to migrate to lymph nodes to transport bacteria.[45] However, whether AMs can egress from the airway and participate in immune responses locally within the lung is unknown. In our study, we find that airway AMs apart from expressing the core macrophage signature genes, also express a unique transcriptional signature. Furthermore, airway AMs upon *Mtb* infection upregulate transcriptional pathways associated with antigen presentation and phagosome maturation. Using a novel IT labeling technique, we show that CCR2^{+} AMs are present within airways during early stages of *Mtb* infection. As the disease progresses, airway AMs can likely respond to chemokine signals from lung epithelial cells (and other cells such as DCs) and egress from the airway and localize within TB granulomas. Upon localization within granulomas, non-airway AMs can undergo classical activation including the production of iNOS, upregulation of genes associated with inflammation, pattern recognition receptors, and T cell costimulation thereby providing optimal *Mtb* control. Whether the activation of non-airway AMs is due to localization within the inflammatory granulomas and dependent on signals within the granuloma is yet to be studied.

This airway labeling technique we have developed can be useful in the study of airway-localized immune cell types in the lung, including the localization of AMs, monocytes, DCs, and neutrophils in the airways versus lung tissue. While this labeling technique can be useful for tracking early cellular changes in the airways as in this study, upon formation of granulomas and disease progression to chronic stages of infection, the structural integrity of the lung airway epithelium can be compromised and may be a caveat as airway administered antibody may leak, thus also labeling non-airway cells. Furthermore, with time, fluid accumulation and scarring may occur in the airway, leading to less effective labeling of airway cells. These caveats should be carefully considered in the use of this labeling technique during chronic stages of infection, or under conditions of loss of structural integrity or tissue scarring.

In summary, we show that CCR2 expression, while dispensable for protection against *Mtb* lineage 4 infections, is critical for protection against emerging *Mtb* strains. Together our data show that during early HN878 infection, AMs upregulate CCR2 and accumulate in the airways. As the infection progresses, some AMs remain in the airway where they likely continue to phagocytose and process TB antigen. Other CCR2^{+} AMs egress in response to the production of CCL2 by epithelial cells or DCs around forming granulomas, and interact with other inflammatory cells to become classically activated and potentially localize within organized granulomas to mediate *Mtb* control. Thus, our results provide novel insights into the role of AMs and the CCR2 axis in macrophage anti-microbial mechanisms of protection against *Mtb* infection.

MATERIALS AND METHODS

Mice

C57BL/6J (B6), CCR2$^{-/-}$,[13] and CCL2$^{-/-}$[46] mice on the B6 background were purchased from The Jackson Laboratory (Bar Harbor, ME). CCR2-DTR[34] and CCR2-GFP[33] were a kind gift from Drs. Robyn Klein and Marco Colonna at Washington University School of Medicine and bred in-house. IKK2$^{fl/fl}$ Sftpc-cre[21] were a kind gift from Dr. Pasparakis (University of Cologne). CCR2-DTR mice were administered sterile PBS or 20 ng Dtx/g body weight (VWR, Radnor, PA) approximately 500 ng/mouse in 200 µL sterile PBS, intraperitoneally (IP), 3 times as indicated.

All mice were maintained in the animal facility at Washington University in St. Louis and bred in-house. Experimental mice were age and sex matched and infected between the ages of 6 and 8 weeks. All mice were maintained and used in accordance with the approved Washington University in St. Louis Institutional Animal Care and Use Committee guidelines. Both male and female

mice were used and to our knowledge no sex-based differences were observed.

Mtb strains and experimental infections

Mtb strains H37Rv (Trudeau Institute), CDC1551, HN878, and HN563 were obtained from BEI Resources (Manassas, VA) under National Institutes of Health contract AI-75320. HN878 *pks1-15*::*hygB* was used as previously published.[6] H37Rv-GFP and HN878-GFP was transformed with the integrating EGFP expression vector pMV261.kan (provided by Dr. Christina Stallings, Washington University in St. Louis) to generate GFP-expressing *Mtb*. Indo-Oceanic T17x strain was acquired from Dr. Karen M. Dobos, Colorado State University. All *Mtb* strains were cultured in Proskauer Beck medium supplemented with 0.05% Tween 80 and frozen at −80 °C while in mid-log phase. Mice were aerosol-infected with low doses (~100 CFU) of indicated *Mtb* strains in sterile PBS using a Glass-col nebulizer.[47] Mice were monitored and weighed as needed and lungs and spleens were harvested at described time points. *Mtb* CFU/organ was quantitated by plating serial dilutions of homogenized lung or spleen tissue on 7H11 agar plates (BD Biosciences, Franklin Lakes, NJ). Plates were incubated for 2–3 weeks at 37 °C and colonies were counted visually.

In vitro culture of cells

Mouse epithelial C10 cells were cultured in complete Dulbecco's modified eagle's medium (cDMEM) to confluence for approximately 2 days. Counts from a representative well were used to calculate the concentration of C10 cells/well, performed visually by hemocytometer.

Bone marrow-derived macrophages (BMDMs) and bone marrow-derived DCs (BMDCs) were cultured from bone marrow cells as previously described.[48] Briefly, bone marrow cells from the femur and tibia of B6 and gene deficient mice were extracted, and 1×10^7 cells were plated in 10 mL of cDMEM supplemented with 20 ng/mL mouse recombinant (rm) granulocyte-macrophage colony-stimulating factor (GM-CSF) (Peprotech, Rocky Hill, NJ).[47] Cells were then cultured at 37 °C in 5% CO_2. On day 3, 10 mL of cDMEM containing 20 ng/mL rmGM-CSF was added. On day 7, adherent cells were collected as macrophages and non-adherent cells were collected as dendritic cells (DCs).

Chemotaxis assay

BMDMs were grown as above, and plated at 2×10^6/mL and stimulated with 20 µg/mL irradiated HN878 (BEI) for 24 h in cDMEM at 37 °C. BMDMs were then added to the upper chamber of the 24-well transwell plate (Costar, Cambridge, CA), 1×10^5 cells/well in 100 µL of Hank's balanced salt solution containing 1% fetal bovine serum with 600 µL of indicated conditioned media beneath the transwell in a 24-well plate. These were incubated for 90 min at 37 °C, then transmigrated cells were collected from the lower chamber, stained and analyzed by flow cytometry.

In vitro infections

BMDMs, BMDCs, and C10 epithelial cells were infected with *Mtb* (multiplicity of infection, MOI:1) in antibiotic-free cDMEM. Cell culture supernatants were collected for analysis of cytokines 48 h post infection.

Adoptive transfer

Lung cell suspensions were prepared as before from the lungs of donor CCR2-GFP ($^+$/KI or KI/KI) mice on 30 dpi following HN878 infection. $CD11c^+$ cells were enriched from the lung suspension using magnetic selection with CD11c microbeads (Miltenyi Biotec, Auburn, CA) per manufacturer's instructions, yielding a population of (>85%) $CD11c^+$ cells. These cells were resuspended at 1×10^7 cells in 500 µL sterile PBS. 50 µL (1×10^6 cells) of this suspension was administered IT to HN878-infected mice at 30 dpi. These mice were harvested on 50 dpi as indicated.

BMDMs were grown as above, and plated at 2×10^6 cells/mL and stimulated with 20 µg/mL irradiated HN878 (BEI) for 24 h in cDMEM at 37 °C. These cells were then harvested and resuspended at 1×10^7 cells in 500 µL sterile PBS. 50 µL (1×10^6 cells) of this suspension was administered IT to HN878-infected mice at 15 and 22 or 30 dpi as indicated.

Flow cytometry

For distinguishing between airway and non-airway cells, mice received 0.7 µg of V500 or PE-conjugated CD45.2 mAb (Clone 104, BD Biosciences and Biolegend, San Diego, CA), administered IT in 50 µL sterile PBS per mouse. Mice were rested for 15 min following which lungs were harvested. To validate the technique some mice received 50 uL of HCl in sterile water (pH 1.5) intratracheally and rested for 24 h prior to instillation of CD45.2 antibody.[49]

Lung single cell suspensions were prepared as before,[47] treated with Fc Block (CD16/CD32, 2.4G2, Tonbo Biosciences, San Diego, CA), and stained with appropriate fluorochrome-labeled specific antibodies or isotype control antibodies: CD11c (HL3, BD Biosciences), CD11b (M1/70, BD Biosciences and Tonbo Biosciences), SiglecF (E50-2440, BD Biosciences), CD64(X54-5/7.1, Biolegend), Gr-1 (RB6-8C5, BD Biosciences), CCR2 (FAB5538P, R&D Systems), CX3CR1 (SA011F11, Biolegend), Ly6C (AL21, BD Biosciences), Ly6G (1A8, BD Biosciences), CD3 (145-2C11, Tonbo Biosciences), CD4 (GK1.5, BD Biosciences), CD44 (IM7, eBioscience), IFN-γ (XMG1.2, BD Biosciences), and rat IgG1 (BD Biosciences). Cells were processed using a Becton Dickinson FACS LSR Fortessa flow cytometer using FACSDiva software, or sorted on a Becton Dickinson FACSJazz cell sorter using BD FACS sorting software. Cells were gated based on their forward and side scatter characteristics and the frequency of specific cell types was calculated using FlowJo (FlowJo, LLC, Ashland, OR). Neutrophils were defined as $CD11b^+CD11c^-Gr\text{-}1^{hi}$ cells, monocytes were defined as $CD11b^+CD11c^-Gr\text{-}1^{lo}$ cells, and RMs were defined as $CD11b^+CD11c^-Gr\text{-}1^-$ cells. mDCs were defined as $CD11b^+CD11c^+$ cells. AMs were defined as $CD11b^{lo}CD11c^+$ cells (Fig. 1) and subsequently as $CD11b^{lo}CD11c^+SiglecF^+$ cells. The flow cytometry gating strategy used for lung subset analysis was an approach using our IT labeling method to select for airway populations and a combined gating strategy from several previous publications.[36,50–53]

For uptake experiments, lung cell suspensions were prepared from H37Rv-GFP- or HN878-GFP-infected B6 mice and stained with appropriate fluorochrome-labeled specific antibodies. Uptake was determined by the co-localization of GFP with known fluorophore-conjugated cell subset markers as measured by flow cytometry.

Broncho-alveolar lavage (BAL)

Mice were administered IT CD45.2 Ab as above and ~10 min later euthanized. BAL was then performed as previously described.[54,55] Briefly, the chest cavity was opened and the sternum/ribcage was resected. The trachea was isolated and a blunt tipped needle was gently inserted into the trachea. The lungs were lavaged with ~5 (5 × 1 mL) washes with sterile 0.2 mM EDTA (Sigma-Aldrich) in PBS. Cells were collected from these lavages and analyzed by flow cytometry as above.

RNA extraction and quantitative real-time PCR (qRT-PCR)

Lung tissue was homogenized and snap-frozen in RLT buffer (Qiagen, Valencia, CA). Total RNA was extracted from lung tissue using the Qiagen RNeasy Mini kit (Qiagen). RNA was converted to cDNA using ABI reverse transcription reagents (ABI/ThermoFisher Scientific, Carlsbad, CA) using a BioRad DNA Engine Thermal Cycler (BioRad, Hercules, CA). cDNA was then amplified using TaqMan reagents on the ABI Viia7 Real-Time PCR detection system (ThermoFisher Scientific). The primer and probe sequences for murine glyceraldehyde 3-phosphate

dehydrogenase (*Gapdh*) and *Tnfa* were previously published.[56] The primers and probes for murine *Arg1*, *Ccl2*, *Ccl7*, and *Ccl12* were purchased commercially (ABI Biosystems). The primer and probe sequences for *Tgfb1* are forward 5′-TGACGTCACTGG AGTTGTACGG-3′, reverse 5′-GGTTCATGTCATGGATGGTGC-3′, probe 5′-/56-FAM/TTC AGC GCT CAC TGC TCT TGT GAC AG/ 3BHQ_1/-3′. Fold increase was determined over uninfected controls relative to *Gapdh* expression using the ΔΔCT calculation as previously described.[56]

RNA-sequencing of AM populations

AMs were sorted and RNA was extracted as described above. RNA sequencing libraries were generated using Clontech SMART-Seq v4 Ultra Low Input RNA Kit for sequencing and Illumina Nextera XT DNA Library preparation kit following the manufacturer's protocol. The cDNA libraries were validated using KAPA Biosystems primer premix kit with Illumina-compatible DNA primers and quality was examined using Agilent Tapestation 2200. The cDNA libraries were pooled at a final concentration of 1.8 pM. Cluster generation and 75 bp paired-read dual-indexed sequencing were performed on Illumina NextSeq 500. Single-ended 75 bp reads were cleaned using Trimmomatic (version 0.36) to remove adapters and quality trimmed to filter out reads <60 bp in length (after trimming). Cleaned sequence data was mapped against the mouse reference genome build GRCh38.90 (Ensembl) using the HISAT2[57] aligner (version 2.1.0) with default parameters, generating sam format alignment files. These sam files were then used as input for featureCounts (version 1.5.1), requiring a minimum mapping quality score of 10. Raw read counts were used as input for DESeq2[26] (version 1.16.1) differential expression analysis, using default settings and an FDR-adjusted *P* value threshold of 0.05 for significant differential expression. Lists of differentially expressed genes were used to test for significant enrichment among KEGG pathways[58] and Mammalian Phenotype Ontology,[59] using WebGestalt[60] (default settings, adjusted $P = 0.05$ threshold for enrichment). Heatmap clustering was performed using "hclust" in R, using Pearson distances and complete linkage, based on *Z*-scores calculated per row using Microsoft Excel.

Histology

Lung lobes were perfused with 10% neutral buffered formalin and embedded in paraffin. For immunofluorescent staining, formalin-fixed paraffin-embedded (FFPE) lung sections were cut, immersed in xylene to remove paraffin, and then sequentially hydrated in absolute ethanol, 95% ethanol, 70% ethanol, and water. Antigens were unmasked with a DakoCytomation Target Retrieval Solution (Dako, Carpinteria, CA) and nonspecific binding was blocked with 5% (v/v) normal donkey serum and Fc Block (BD Pharmingen, San Jose, CA). Endogenous biotin (Sigma-Aldrich) was neutralized by adding avidin followed by incubation with biotin.

Antibodies used for identification of lung cells as previously described:

Rabbit anti-*Mycobacterium tuberculosis* antibody, (MBS534825, MyBiosource.com)

Rabbit anti MCP-1/CCL2 (GTX37379, GeneTex, Irvine, CA)

Goat anti-human/mouse E-Cadherin (AF748, R&D Systems)

Monoclonal hamster anti-ITGAX/CD11c (N418, Lifespan Biosciences, Inc., Seattle, WA)

Polyclonal rabbit anti-Siglec 5/CD170 (LS-C97825, Lifespan Biosciences, Inc.). Fluorescein (FITC) affinipure $F(ab')_2$ fragment donkey anti-rabbit IgG (H^+L) (711-096-152, Jackson Immunoresearch, West Grove, PA).

Biotin-SP (long spacer) affinipure $F(ab')_2$ fragment rabbit anti-Syrian hamster IgG (H^+L) (307-066-003, Jackson Immunoresearch).

Streptavidin, Alexa Fluor® 488 conjugate (S-11223, ThermoFisher Scientific).

Biotinylated goat anti-GFP (GTX26658, Genetex, Irvine, CA) was visualized with Alexa Fluor 568 donkey anti-goat IgG and Alexa Fluor 555 streptavidin. GFP stain was pseudocolored to green with the Axiovision software. Images were collected using an inverted Observer.Z1 Axioplan Zeiss Microscope with Colibri system (Zeiss, Thornwood, NY) and the Axiovision Rel 4.8. Software.

FFPE lung sections were stained with hematoxylin and eosin (H&E) and inflammatory features were evaluated by light microscopy. Inflammatory lesions were outlined with the automated tool of the Zeiss Axioplan 2 microscope (Carl Zeiss) and percentage of inflammation was calculated by dividing the inflammatory area by the total area of individual lung lobes. FFPE lung sections were stained for collagen and muscle using Masson's Trichrome 2000 stain procedure kit (#KTMTR2, American Mastertech, Lodi, CA) per the manufacturer's instructions. Trichrome stained slide images were acquired using a Hamamatsu Nanozoomer 2.0 HT system with NDP scan image acquisition software. Trichrome staining was quantified using Visiomorph image processing software (Visiopharm, Broomfield, CO). FFPE lung sections were subjected to in situ hybridization (ISH) with the mouse-Ccl2 probe using the RNAscope 2.5HD Detection Kit (Brown staining) as per the manufacturer's recommendations (Advanced Cell Diagnostics, Newark, CA). The representative pictures were taken with the Hamamatsu Nanozoomer 2.0 HT system with NDP scan image acquisition software.

Cytokine production quantification

Cytokine levels within cell culture supernatants were analyzed using the BD OptEIA Mouse CCL2 ELISA kit (BD Biosciences) or using Milliplex Multiplex Assays (Millipore, Billerica, MA), as per standard protocol.

Statistical analyses

Statistical analyses were performed using GraphPad Prism 5 and Microsoft Excel. Specific analysis techniques and post tests are mentioned in figure legends. SEM error bars displayed. $^*P \le 0.05$, $^{**}P \le 0.01$, $^{***}P \le 0.001$, n.s.—not significant.

ACKNOWLEDGEMENTS

This work was supported by Washington University in St. Louis, NIH grant HL105427 to S.A.K., AI111914 and AI134236 to S.A.K. and D.K., NIH/NHLBI T32 AI007172 to M.D.D., NIH/NHLBI T32 HL007317-37 to N.H., and NIH Shared Instrumentation Grant S10 RR0227552. J.R.M. was supported by funds of the Department of Medicine, University of Rochester, and U19 AI91036. The authors thank Drs. Robyn Klein (Washington University in St. Louis) and Marco Colonna (Washington University in St. Louis) for generously providing mice. We thank Dr. Kimberly Thomas for critical reading of the manuscript, Sarah Squires and Lan Lu (Washington University in St. Louis) for technical support, William Horne (University of Pittsburgh) for carrying out RNA sequencing.

AUTHOR CONTRIBUTIONS

N.H., M.D.D., G.J.R. and S.A.K. conceived and designed the experiments, M.D.D., N.H., S. D., O.P., N.S., M.A., J.R.-M., K.K., B.A.R., J.M., M.M., D.K. and G.K. performed the experiments and/or analyzed data and provided reagents, M.D.D. and S.A.K wrote the paper, all authors edited the paper, S.A.K. provided funding and overall project supervision.

ADDITIONAL INFORMATION

The online version of this article (https://doi.org/10.1038/s41385-018-0071-y) contains supplementary material, which is available to authorized users.

Competing interests: The authors declare no competing interests.

REFERENCES

1. World Health Organization. (2016) . Global tuberculosis report 2016. World Health Organization. http://www.who.int/iris/handle/10665/250441
2. Scott, H. M. & Flynn, J. L. *Mycobacterium tuberculosis* in chemokine receptor 2-deficient mice: influence of dose on disease progression. *Infect. Immun.* **70**, 5946–5954 (2002).
3. Samstein, M. et al. Essential yet limited role for CCR2(+) inflammatory monocytes during *Mycobacterium tuberculosis*-specific T cell priming. *eLife* **2**, e01086 (2013).
4. Domingo-Gonzalez, R., Prince, O., Cooper, A. & Khader, S. A. Cytokines and chemokines in *Mycobacterium tuberculosis* infection. *Microbiol. Spectr.* **4**, https://doi.org/10.1128/microbiolspec.TBTB2-0018-2016 (2016).
5. Tian, G., Li, X., Li, H., Wang, X. & Cheng, B. Systematic meta-analysis of the association between monocyte chemoattractant protein-1 −2518A/G polymorphism and risk of tuberculosis. *Genet. Mol. Res.* **14**, 5501–5510 (2015).
6. Reed, M. B. et al. A glycolipid of hypervirulent tuberculosis strains that inhibits the innate immune response. *Nature* **431**, 84–87 (2004).
7. Gopal, R. et al. Unexpected role for IL-17 in protective immunity against hypervirulent *Mycobacterium tuberculosis* HN878 infection. *PLoS Pathog.* **10**, e1004099 (2014).
8. Cambier, C. J. et al. Mycobacteria manipulate macrophage recruitment through coordinated use of membrane lipids. *Nature* **505**, 218–222 (2014).
9. Cambier, C. J., O'Leary, S. M., O'Sullivan, M. P., Keane, J. & Ramakrishnan, L. Phenolic glycolipid facilitates mycobacterial escape from microbicidal tissue-resident macrophages. *Immunity*. https://doi.org/10.1016/j.immuni.2017.08.003 (2017).
10. Armstrong, J. A. & Hart, P. D. Phagosome–lysosome interactions in cultured macrophages infected with virulent tubercle bacilli. Reversal of the usual non-fusion pattern and observations on bacterial survival. *J. Exp. Med.* **142**, 1–16 (1975).
11. Srivastava, S., Ernst, J. D. & Desvignes, L. Beyond macrophages: the diversity of mononuclear cells in tuberculosis. *Immunol. Rev.* **262**, 179–192 (2014).
12. Antonelli, L. R. et al. Intranasal poly-IC treatment exacerbates tuberculosis in mice through the pulmonary recruitment of a pathogen-permissive monocyte/macrophage population. *J. Clin. Invest.* **120**, 1674–1682 (2010).
13. Peters, W. et al. Chemokine receptor 2 serves an early and essential role in resistance to *Mycobacterium tuberculosis*. *Proc. Natl Acad. Sci. USA* **98**, 7958–7963 (2001).
14. Gagneux, S. & Small, P. M. Global phylogeography of *Mycobacterium tuberculosis* and implications for tuberculosis product development. *Lancet Infect. Dis.* **7**, 328–337 (2007).
15. Serbina, N. V., Shi, C. & Pamer, E. G. Monocyte-mediated immune defense against murine Listeria monocytogenes infection. *Adv. Immunol.* **113**, 119–134 (2012).
16. Eruslanov, E. B. et al. Neutrophil responses to *Mycobacterium tuberculosis* infection in genetically susceptible and resistant mice. *Infect. Immun.* **73**, 1744–1753 (2005).
17. Lowe, D. M. et al. Neutrophilia independently predicts death in tuberculosis. *Eur. Respir. J.* **42**, 1752–1757 (2013).
18. Lowe, D. M., Redford, P. S., Wilkinson, R. J., O'Garra, A. & Martineau, A. R. Neutrophils in tuberculosis: friend or foe? *Trends Immunol.* **33**, 14–25 (2012).
19. Yeremeev, V., Linge, I., Kondratieva, T. & Apt, A. Neutrophils exacerbate tuberculosis infection in genetically susceptible mice. *Tuberculosis (Edinb.)* **95**, 447–451 (2015).
20. Vasquez-Loarte, T., Trubnykova, M. & Guio, H. Genetic association meta-analysis: a new classification to assess ethnicity using the association of MCP-1 −2518 polymorphism and tuberculosis susceptibility as a model. *BMC Genet.* **16**, 128 (2015).
21. Pasparakis, M. et al. TNF-mediated inflammatory skin disease in mice with epidermis-specific deletion of IKK2. *Nature* **417**, 861–866 (2002).
22. Wang, J., Gigliotti, F., Bhagwat, S. P., Maggirwar, S. B. & Wright, T. W. Pneumocystis stimulates MCP-1 production by alveolar epithelial cells through a JNK-dependent mechanism. *Am. J. Physiol. Lung Cell Mol. Physiol.* **292**, L1495–L1505 (2007).
23. Misharin, A. V. et al. Monocyte-derived alveolar macrophages drive lung fibrosis and persist in the lung over the life span. *J. Exp. Med.* **214**, 2387–2404 (2017).
24. Gautier, E. L. et al. Systemic analysis of PPARgamma in mouse macrophage populations reveals marked diversity in expression with critical roles in resolution of inflammation and airway immunity. *J. Immunol.* **189**, 2614–2624 (2012).
25. Huang, L., Nazarova, E. V., Tan, S., Liu, Y. & Russell, D. G. Growth of *Mycobacterium tuberculosis* in vivo segregates with host macrophage metabolism and ontogeny. *J. Exp. Med.* **215**, 1135–1152 (2018).
26. Love, M. I., Huber, W. & Anders, S. Moderated estimation of fold change and dispersion for RNA-seq data with DESeq2. *Genome Biol.* **15**, 550 (2014).
27. Roy, S. et al. Batf2/Irf1 induces inflammatory responses in classically activated macrophages, lipopolysaccharides, and mycobacterial infection. *J. Immunol.* **194**, 6035–6044 (2015).
28. Xu, H. et al. Notch-RBP-J signaling regulates the transcription factor IRF8 to promote inflammatory macrophage polarization. *Nat. Immunol.* **13**, 642–650 (2012).
29. Mass, E. et al. Specification of tissue-resident macrophages during organogenesis. *Science.* **353**, https://doi.org/10.1126/science.aaf4238 (2016).
30. de Jager, S. C. et al. Growth differentiation factor 15 deficiency protects against atherosclerosis by attenuating CCR2-mediated macrophage chemotaxis. *J. Exp. Med.* **208**, 217–225 (2011).
31. Hu, J. et al. Polo-like kinase 1 (PLK1) is involved in toll-like receptor (TLR)-mediated TNF-alpha production in monocytic THP-1 cells. *PLoS ONE* **8**, e78832 (2013).
32. Lyu, J. H., Huang, B., Park, D. W. & Baek, S. H. Regulation of PHLDA1 expression by JAK2-ERK1/2-STAT3 signaling pathway. *J. Cell. Biochem.* **117**, 483–490 (2016).
33. Satpathy, A. T. et al. Notch2-dependent classical dendritic cells orchestrate intestinal immunity to attaching-and-effacing bacterial pathogens. *Nat. Immunol.* **14**, 937–948 (2013).
34. Hohl, T. M. et al. Inflammatory monocytes facilitate adaptive CD4 T cell responses during respiratory fungal infection. *Cell Host Microbe* **6**, 470–481 (2009).
35. Domingo-Gonzalez, R. et al. Interleukin-17 limits hypoxia-inducible factor 1 alpha and development of hypoxic granulomas during tuberculosis. *JCI Insight*. **2**, https://doi.org/10.1172/jci.insight.92973 (2017).
36. Davies, L. C., Jenkins, S. J., Allen, J. E. & Taylor, P. R. Tissue-resident macrophages. *Nat. Immunol.* **14**, 986–995 (2013).
37. Schorey, J. S. & Schlesinger, L. S. Innate immune responses to tuberculosis. *Microbiol. Spectr.* **4**, https://doi.org/10.1128/microbiolspec.TBTB2-0010-2016 (2016).
38. Arbues, A., Lugo-Villarino, G., Neyrolles, O., Guilhot, C. & Astarie-Dequeker, C. Playing hide-and-seek with host macrophages through the use of mycobacterial cell envelope phthiocerol dimycocerosates and phenolic glycolipids. *Front. Cell. Infect. Microbiol.* **4**, 173 (2014).
39. Dutta, N. K. et al. The stress-response factor SigH modulates the interaction between *Mycobacterium tuberculosis* and host phagocytes. *PLoS ONE* **7**, e28958 (2012).
40. Flores-Villanueva, P. O. et al. A functional promoter polymorphism in monocyte chemoattractant protein-1 is associated with increased susceptibility to pulmonary tuberculosis. *J. Exp. Med.* **202**, 1649–1658 (2005).
41. Hussell, T. & Bell, T. J. Alveolar macrophages: plasticity in a tissue-specific context. *Nat. Rev. Immunol.* **14**, 81–93 (2014).
42. Brace, P. T. et al. *Mycobacterium tuberculosis* subverts negative regulatory pathways in human macrophages to drive immunopathology. *PLoS Pathog.* **13**, e1006367 (2017).
43. Cumming, B. M. et al. *Mycobacterium tuberculosis* arrests host cycle at the G(1)/S transition to establish long term infection. *PLoS Pathog.* **13**, e1006389 (2017).
44. Koo, M.-S., Subbian, S. & Kaplan, G. Strain specific transcriptional response in *Mycobacterium tuberculosis* infected macrophages. *Cell Commun. Signal.* **10**, 2 (2012).
45. Kirby, A. C., Coles, M. C. & Kaye, P. M. Alveolar macrophages transport pathogens to lung draining lymph nodes. *J. Immunol.* **183**, 1983–1989 (2009).
46. Lu, B. et al. Abnormalities in monocyte recruitment and cytokine expression in monocyte chemoattractant protein 1-deficient mice. *J. Exp. Med.* **187**, 601–608 (1998).
47. Khader, S. A. et al. IL-23 and IL-17 in the establishment of protective pulmonary CD4+ T cell responses after vaccination and during *Mycobacterium tuberculosis* challenge. *Nat. Immunol.* **8**, 369–377 (2007).
48. Lin, Y. et al. Interleukin-17 is required for T helper 1 cell immunity and host resistance to the intracellular pathogen *Francisella tularensis*. *Immunity* **31**, 799–810 (2009).
49. Eickmeier, O. et al. Altered mucosal immune response after acute lung injury in a murine model of Ataxia Telangiectasia. *BMC Pulm. Med.* **14**, 93 (2014).
50. Desvignes, L., Wolf, A. J. & Ernst, J. D. Dynamic roles of type I and type II IFNs in early infection with *Mycobacterium tuberculosis*. *J. Immunol.* **188**, 6205–6215 (2012).
51. Misharin, A. V., Morales-Nebreda, L., Mutlu, G. M., Budinger, G. R. & Perlman, H. Flow cytometric analysis of macrophages and dendritic cell subsets in the mouse lung. *Am. J. Respir. Cell Mol. Biol.* **49**, 503–510 (2013).
52. Bedoret, D. et al. Lung interstitial macrophages alter dendritic cell functions to prevent airway allergy in mice. *J. Clin. Invest.* **119**, 3723–3738 (2009).
53. Jakubzick, C. et al. Minimal differentiation of classical monocytes as they survey steady-state tissues and transport antigen to lymph nodes. *Immunity* **39**, 599–610 (2013).
54. Gopal, R. et al. S100A8/A9 proteins mediate neutrophilic inflammation and lung pathology during tuberculosis. *Am. J. Respir. Crit. Care Med.* **188**, 1137–1146 (2013).
55. Slight, S. R. et al. CXCR5(+) T helper cells mediate protective immunity against tuberculosis. *J. Clin. Invest.* **123**, 712–726 (2013).
56. Khader, S. A. et al. IL-23 compensates for the absence of IL-12p70 and is essential for the IL-17 response during tuberculosis but is dispensable for protection and antigen-specific IFN-gamma responses if IL-12p70 is available. *J. Immunol.* **175**, 788–795 (2005).

57. Kim, D., Langmead, B. & Salzberg, S. L. HISAT: a fast spliced aligner with low memory requirements. *Nat. Methods* **12**, 357–360 (2015).
58. Kanehisa, M., Sato, Y., Kawashima, M., Furumichi, M. & Tanabe, M. KEGG as a reference resource for gene and protein annotation. *Nucleic Acids Res.* **44**, D457–D462 (2016).
59. Smith, C. L. & Eppig, J. T. The Mammalian Phenotype Ontology as a unifying standard for experimental and high-throughput phenotyping data. *Mamm. Genome* **23**, 653–668 (2012).
60. Zhang, B., Kirov, S. & Snoddy, J. WebGestalt: an integrated system for exploring gene sets in various biological contexts. *Nucleic Acids Res.* **33**, W741–W748 (2005).